JACS
JOURNAL OF THE AMERICAN CHEMICAL SOCIETY

ARTICLE

pubs.acs.org/JACS

Surface-Amplified Ligand Disorder in CdSe Quantum Dots Determined by Electron and Coherent Vibrational Spectroscopies

Matthew T. Frederick, Jennifer L. Achtyl, Kathryn E. Knowles, Emily A. Weiss,* and Franz M. Geiger*

Department of Chemistry, Northwestern University, 2145 Sheridan Road, Evanston, Illinois 60208-3113, United States

Supporting Information

ABSTRACT: This Article reports measurements of the intra- and intermolecular ordering of tight-binding octylphosphonate ligands on the surface of colloidal CdSe quantum dots (QDs) within solid state films, and the dependence of this order on the size of the QDs. The order of the organic ligands, as probed by vibrational sum frequency generation (SFG) spectroscopy, decreases as the radius of the QDs decreases; this decrease is correlated with a decrease in the order of underlying Cd^{2+}, as detected by X-ray photoelectron spectroscopy (XPS) line width measurements, for radii of the QDs, $R > 2.4$ nm, and is independent of the disorder of the Cd^{2+} for $R < 2.4$ nm. We believe that, for $R < 2.4$, the decreasing order of the ligands with decreasing size is due to an increase in the curvature of the QD surfaces. Disorder in the Cd^{2+} results from the presence of a shell of Cd^{2+}−surfactant complexes that form during synthesis, so this work demonstrates the possibility for chemical control over molecular order within films of colloidal QDs by changing the surfactant mixture.

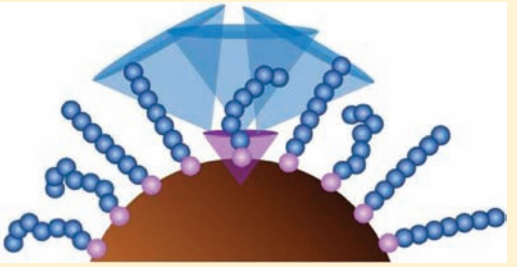

INTRODUCTION

This Article describes a study of the correlation between the intra- and intermolecular order of *n*-octylphosphonate ligands bound to CdSe quantum dots (QDs) and (i) the radius, *R*, of the QDs, and (ii) the order of the cadmium ions (Cd^{2+}) on their surfaces. The surface chemistry of colloidal QDs has direct implications for their application in energy conversion devices.[1−8] Within such applications, QDs must exchange charge carriers (electrons or holes), created either by photoexcitation or by injection, with proximate QDs, electrodes, or complementary active materials. The kinetics of interfacial charge transfer in QD-based materials are governed by the degree of passivation of charge-trapping surface defects and the height and shape of the tunneling barriers created by passivating ligands.[9−13] The structural ordering of the ligands on the QD surfaces is a critical observable relevant to both of these parameters.[14]

We and others[15−17] have had some success in structurally and chemically characterizing the QD−ligand interface (in particular, measuring QD−ligand association constants) in solution, but these measurements do not directly yield information about the intermolecular structure of ligand monolayers on QD surfaces within films; this information is necessary to map ligand ordering to macroscopic observables such as conductivity. Several groups have measured the intermolecular order of monolayers of alkyl ligands within films of metal nanoparticles[18−20] and nanostructured silica[21] using NMR,[18] DSC,[19] and FTIR.[19−21] These studies establish that the principles that apply to cooperative effects among alkyl ligands on flat surfaces, such as that the driving force for crystalline packing and formation of all-trans conformations is proportional to alkyl chain length, also apply to monolayers on high-curvature surfaces, but that increasing the curvature of the substrate induces disordering in the monolayer in the form of gauche defects.

This study provides an unprecedented view of size-dependent order of both organic and inorganic components at the QD−surfactant interfaces of nanocrystals of a compound semiconductor, a system that is chemically more complex than metal nanoparticles. We apply symmetry-sensitive vibrational sum frequency generation (SFG) to determine the molecular order within layers of *n*-octylphosphonate (OPA) ligands on colloidal CdSe QDs; this order is indicated by the ratio of trans-extended alkyl chains to chains containing gauche defects. We find that the degree of order within the OPA layer decreases as the radius of the QDs decreases from 3.0 to 2.0 nm. Two factors appear to dictate this order: (i) As the size of the QDs decreases, the curvature of their surfaces increases. This increase leads to an increase available cone volume for each ligand,[22] and a decrease in the domain size available for packing of the ligands,[23] both of which facilitate the formation of gauche defects. (ii) As the size of the QDs decreases, the set of geometries and chemical environments of the underlying surface cadmium ions becomes more heterogeneous. We measure this heterogeneity by the line width of the cadmium peaks within the X-ray photoelectron (XP) spectra of the QDs. Factor (ii) arises because we synthesize the QDs with a very common procedure[24] that uses reagent grade trioctylphosphine oxide (TOPO) as the coordinating solvent. We[25,26] and others[27] have shown previously that the OPA impurities in TOPO drive a cadmium enrichment of QD surfaces in the form of a disordered Cd^{2+}−OPA network around the nanocrystalline

Received: January 17, 2011
Published: April 22, 2011

dx.doi.org/10.1021/ja200466z | *J. Am. Chem. Soc.* 2011, 133, 7476–7481

core (with a ratio Cd/Se = 1:1), and that the degree of cadmium enrichment, and the Cd/Se ratio, increases as R decreases.

Here, we provide evidence, using a combination of XPS and SFG, that the disorder in the surface Cd^{2+} is directly attributable to the presence of this Cd^{2+}−OPA network (factor (ii)) over the range of R we studied, while the disorder in the surface OPA ligands is mainly attributable to the Cd^{2+}−OPA network (factor (ii)) for $R > \sim 2.4$ nm, and to the change in the curvature of the QD surfaces (factor (i)) for $R < \sim 2.4$ nm.

EXPERIMENTAL METHODS

Synthesis of CdSe Quantum Dots. We synthesized colloidal CdSe QDs using the organometallic precursor-based procedure of Qu et al. with minor modifications.[24] We used all reagents and purification solvents, including trioctylphosphine oxide (TOPO), trioctylphosphine (TOP), selenium shot, hexadecylamine (HDA), hexanes, and methanol, as-received from Aldrich, except cadmium stearate, which we used as-received from MP Biomedicals, Inc. We added TOPO (1.94 g, 5.02 mmol), HDA (1.94 g, 8.03 mmol), and cadmium stearate (0.112 g, 0.165 mmol) to a dry 50 mL three-neck round-bottom flask and heated the mixture to 320 °C with stirring under positive nitrogen flow. After the cadmium stearate completely dissolved to form an optically clear solution, we rapidly injected trioctylphosphine selenide (TOPSe, 1 mL of 1 M solution in TOP, prepared and stored in a glovebox). We arrested the growth of the QDs by cooling the reaction with 10 mL of chloroform either immediately after TOPSe injection (for the smallest QDs), after the reaction had cooled to 220 °C (for slightly larger QDs), or after holding the reaction at 290 °C for several minutes, and then cooling to 220 °C (for the largest QDs).

As mentioned in the Introduction, the purity of the TOPO reagent determined the degree of cadmium enrichment in the QDs. Use of 90% TOPO in the procedure described above resulted in QDs with Cd/Se ratios between 1:1 and 5:1 depending on the radius of the QD. Use of 99% TOPO resulted in QDs with Cd/Se ratios between 1:1 and 1.5:1 over the same range of radii. The purity of the TOPO also affected the rate of the growth of the QDs in the synthetic reaction mixture. For the QDs synthesized with 90% TOPO, formation of the largest QDs (~3.7 nm radius) required growth at 290 °C for 20 min. For QDs synthesized with 99% TOPO, formation of the QDs with a 3.7 nm radius required growth at 290 °C for only 4 min.

Purification of QDs. Once the solution cooled to room temperature, we added 20 mL of methanol and centrifuged the mixture (at 3500 rpm for 5 min) to precipitate the QDs. We dispersed the resulting pellet in 10 mL of hexanes and centrifuged again. We collected the supernatant and allowed it to sit for 24 h in the dark, during which time a white precipitate (excess cadmium stearate, TOPO, and HDA) formed. Centrifugation of this suspension produced a white pellet of free ligand, which we discarded, and a colored supernate that contained the QDs. Addition of methanol to this supernate (2:1 by volume) and further centrifugation produced a colored pellet of QDs and colorless supernate containing excess HDA and TOPO. We discarded the supernate and redispersed the pellet in chloroform. We repeated the methanol precipitation step, dried the resulting QD pellet with a stream of nitrogen, and dispersed it in 10 mL of hexanes. We centrifuged the hexanes solution and collected a very small white pellet of free ligand. We stored the supernatant in the dark until use. The sample of CdSe QDs produced with 99% TOPO underwent some precipitation of QDs during the purification process, which we observed as color in the normally white ligand pellets.

SFG Spectroscopy. Detailed descriptions of the theoretical and experimental aspects of sum frequency generation (SFG) are available elsewhere,[30] and our specific optical setup has been described previously.[36] Briefly, the current studies were carried out using an 800 nm 120 fs regeneratively amplified Ti:Sapphire system (Hurricane, Spectra-Physics). The Hurricane system pumps an optical parametric amplifier (OPA-800CF, Spectra Physics) to produce IR light around 3.4 μm with a bandwidth (full width at half-maximum) of ~140 cm^{-1}. The energy of the incident infrared and visible light fields is measured using an energy meter (EPM1000-0110L99, Molectron) and is set to 1.2 μJ for the infrared and to 6 μJ for the visible light fields as these incident energies produced SFG signals that followed the proper dependence on input energy. The IR beam passes through an IR waveplate (L/2 $CdGaS_4$ 3.1 μm CA 10 mm, Altechna Co. Ltd.), before being overlapped with the visible beam and focused onto the surface under investigation, after which the SFG signal was collected with a 0.5 m spectrograph (Acton Research) and detected with a CCD camera (Roper Scientific). Following the work of Esenturk and Walker,[37] we recorded broadband SFG spectra with four different input IR center frequencies to ensure that all vibrational modes in the C−H frequency region were probed. The spectra presented in this work are collected within 1−5 min. The signal normalization and summing procedures are described in our previous work.[38] The SFG spectra were fit using a custom-written Igor Pro software procedure that convolutes Lorentzians. This procedure allows for vibrational modes to be either in or out of phase, that is, 0° or 180°, and includes a term to account for the relatively small nonresonant contribution. As in earlier work,[39] all spectra are referenced to the 2955 cm^{-1} C−H symmetric stretch of the methoxy groups in PMMA. We note that SFG spectra of QDs larger than those studied in this work contained considerable amounts of background from fluorescence bands.

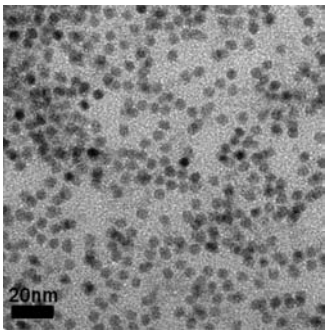

Figure 1. Transmission electron micrograph of CdSe QDs with a radius of 2.3 nm; scale bar = 20 nm.

RESULTS AND DISCUSSION

Characterization of the CdSe QDs. Figure 1 shows a TEM image of CdSe QDs with $R = 2.3$ nm. The standard deviation of R measured by TEM and the full-width at half-maximum (fwhm) of optical emission peaks both indicate that the QDs have diameters with a dispersity of 7−10%. The wavelength of the first excitonic absorption of the QDs increases from 536 to 602 nm as R increases from 2.0 to 3.0 nm (see the Supporting Information for absorption and emission spectra). We note that, due to the cadmium enrichment of some of the QDs, there is a discrepancy between the radii of the QDs we measure by TEM, and the radius predicted by the absorption spectra of the QDs; specifically, the radii we measure for our QDs are consistently ~0.6 nm larger than that predicted by Peng.[26,40]

Previous[25] XPS and ^{31}P NMR studies on CdSe QDs prepared with the same synthetic and purification procedure used in this work (with 90% TOPO as the coordinating solvent) show that these QDs are passivated exclusively by OPA and P'-P'-(di-n-octyl) pyrophosphonate (PPA), the self-condensation product of OPA (Chart 1). We confirmed this result for the QDs used in this

dx.doi.org/10.1021/ja200466z | J. Am. Chem. Soc. 2011, 133, 7476–7481

Chart 1. Chemical Structures of the Organic Ligands on the Surfaces of CdSe QDs Produced with Reagent-Grade (90%) TOPO

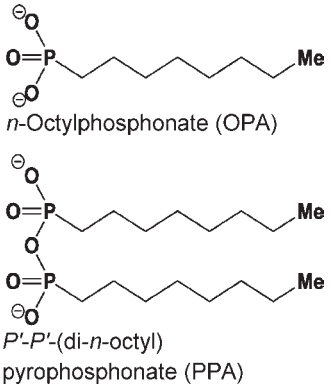

study (see the Supporting Information). The OPA and PPA ligands survive the repeated precipitations used to separate the QDs from excess synthetic reactants because they form multidentate coordinations to Cd^{2+} ions as negatively charged phosphonates, whereas the other major surfactants present during the synthesis, TOPO, TOPSe, and hexadecylamine, coordinate weakly to Cd^{2+} as neutral molecules via dative bonds and are ultimately removed from the QDs during the repeated precipitation steps.

XPS: The Ordering of Cd^{2+} on the QD Surface Depends on the Stoichiometry of the Surface. Figure 2A shows the Cd $3d_{5/2}$ region within representative XP spectra for two sizes of QDs (R = 2.0 nm and R = 3.1 nm) synthesized with 90% TOPO (and therefore passivated by a layer of OPA and PPA). The Cd $3d_{5/2}$ peak for the smaller QDs has a larger binding energy (406.0 eV) and fwhm (1.67 eV) than does the Cd $3d_{5/2}$ peak for the larger QDs (BE = 405.3 eV, fwhm = 1.16 eV). Figure 3A shows that, for the eight sizes of 90% TOPO QDs we studied (black symbols), the fwhm of the Cd $3d_{5/2}$ peak decreases approximately linearly as the radius of the QDs increases. The linewidths of the Cd $3d_{3/2}$ (~412 eV) peaks show the same trend (see the Supporting Information). Figure 3B (black symbols) plots the same XPS linewidths versus the Cd/Se ratio, as measured directly with inductively coupled atomic emission spectroscopy (ICP-AES) or extrapolated from a calibration of curve of Cd/Se ratio versus R that we constructed previously with ICP-AES. These data indicate that, as the radius of the QDs decreases and the degree of cadmium enrichment of their surfaces increases, the heterogeneity of the chemical environments of the Cd^{2+} increases.

Comparing the black symbols in Figure 3A and B does not clarify whether it is the radius of the QD or the cadmium enrichment of the QD that is more directly correlated with the disorder in the Cd^{2+} ions. We therefore synthesized three samples of QDs using, as a coordinating surfactant, 99% TOPO rather than 90% TOPO. Using 99% TOPO significantly decreases or eliminates the cadmium enrichment on the surfaces of the QDs because it contains little or none of the OPA impurity;[26] the QDs synthesized with 99% TOPO are stabilized rather by stearate (the ligand for the Cd^{2+} precursor) and hexadecylamine.[25] The red symbols in Figure 3A indicate the XPS linewidths of the CdSe QDs produced with 99% TOPO. These data do not lie along the same trendline as the black symbols in Figure 3A; for a given size, the Cd^{2+} ions in the QDs produced with 99% TOPO are more ordered than in the QDs produced with 90% TOPO.

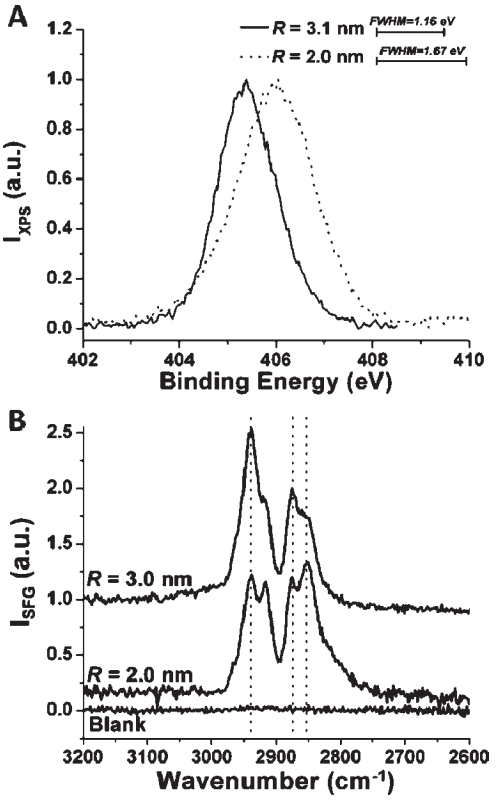

Figure 2. (A) Representative normalized XP spectra of the Cd $3d_{5/2}$ region for CdSe QDs with R = 2.0 nm and R = 3.1 nm drop-cast onto an Si/SiO_2 wafer. (B) Representative SFG spectra, normalized to the maximum SFG intensity at 2875 cm^{-1}, of CdSe QDs with R = 2.0 nm and R = 3.0 nm, spun-cast onto a glass slide, and of a glass slide after evaporation of the hexane solvent (no QDs, "blank"). Vertical dashed lines indicate the CH_3 asymmetric (left) and symmetric (middle) stretches and the CH_2 symmetric stretch (right).

The data from the two types of QDs, however, do lie along the same trendline in Figure 3B, where we plot XPS line width versus Cd/Se ratio. This result indicates that it is Cd/Se ratio, and not radius, that is directly correlated with the order of the Cd^{2+} ions in these QDs, and that the radius is probably correlated with the order through Cd/Se ratio. We believe that the mechanism for the dependence of the XPS line width on Cd/Se ratio is that the Cd^{2+}—ligand complexes that result in the cadmium enrichment (Cd^{2+}—OPA in the 90% TOPO QDs and Cd^{2+}—stearate in the 99% TOPO QDs) adhere to the surface of the QDs with many different geometries and binding motifs. For instance, in the 90% TOPO QDs, some Cd^{2+} ions bind to both OPA and Se^{2-}, and some Cd^{2+} bind to surface-bound OPA without forming any Cd—Se bonds. This variety of binding motifs creates dispersion in cadmium oxidation states and broadens the corresponding peaks in the Cd XP spectrum. The more stoichiometric is the surface of the QDs, the fewer possible binding motifs exist, and the narrower are the peaks in the Cd XP spectrum.

The blue data points in Figures 3A,B indicate the linewidths of the Cd $3d_{5/2}$ peaks of QDs synthesized with 99% TOPO, and subsequently exposed to ambient conditions (in their hexane solution) for 3 weeks before deposition of the XPS samples, during which time the less-passivated QDs precipitated from the sample. The more-passivated QDs that were left in solution had a higher average Cd/Se ratio than that of the freshly prepared

dx.doi.org/10.1021/ja200466z | J. Am. Chem. Soc. 2011, 133, 7476–7481

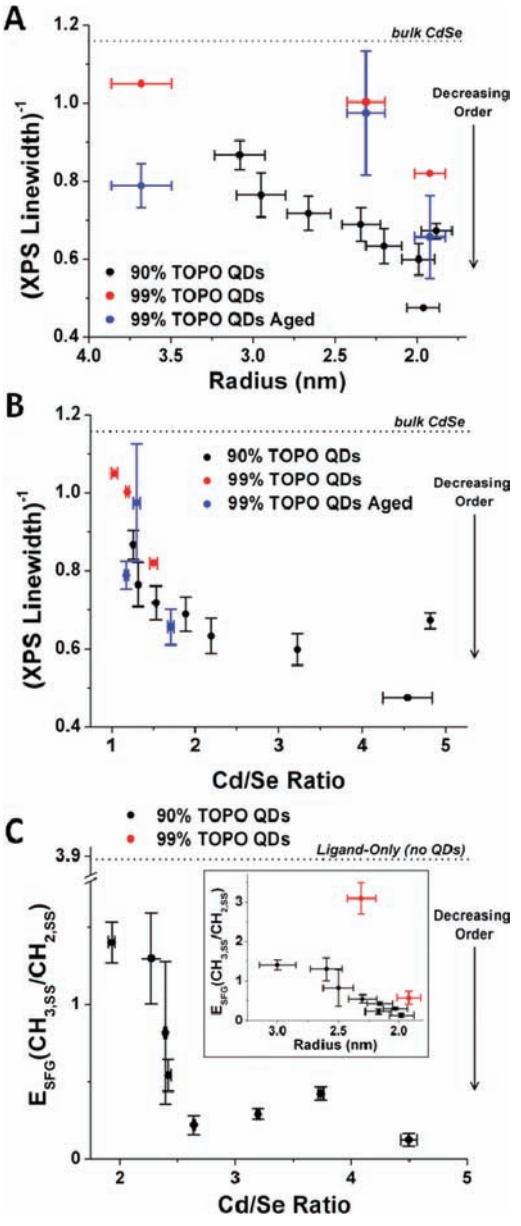

Figure 3. (A,B) Linewidth (fwhm) of the Cd $3d_{5/2}$ peak within XP spectra of samples of CdSe QDs, synthesized with either 90% TOPO (black) or 99% TOPO (red, blue), plotted against the radius of the QDs (A) and the Cd/Se ratio of the QDs (B). The vertical error bars are the standard deviations of at least four measurements on two spots on each of two separately prepared samples. The dashed horizontal lines indicate the line width of the Cd $3d_{5/2}$ peak for bulk CdSe. We prepared the "aged" samples (blue) for XPS as described in the text. (C) Ratio of the SFG amplitudes, *E*, of CH_3 and CH_2 symmetric stretches from the ligands on the CdSe QDs, synthesized with either 90% TOPO (black) or 99% TOPO (red), plotted against the Cd/Se ratio and radius (inset) of the QDs. The vertical error bars are the standard deviations of four measurements on one sample. The dashed horizontal line indicates the SFG ratio for OPA ligands spun-cast onto glass slides from hexanes. The horizontal error bars in (A) are the uncertainty in the radius of the QD ($\sim\pm5\%$), as measured by the line width of their PL spectra. The horizontal error bars in (B,C) are the standard deviations of the Cd/Se ratio, determined by measuring three separately prepared ICP-AES samples. For data points with no horizontal error bars, we extrapolated the Cd/Se ratio from a previously constructed calibration curve of Cd/Se ratio versus *R* (ref 26).

sample because tightest binding, most stabilizing surfactant molecules bind preferentially to Cd^{2+} (not Se^{2-}). The degree of disorder in the Cd^{2+} ions in these aged, more cadmium-enriched 99% TOPO samples (Figure 3A, blue symbols) was higher than that of the freshly prepared 99% TOPO samples (red symbols), such that these data points, too, lie along the trendline when we plot line width versus Cd/Se ratio in Figure 3B. We note that no such precipitation occurred in the samples of QDs produced with 90% TOPO, and the XPS linewidths for samples prepared from freshly synthesized QDs using 90% TOPO are the same as those for samples prepared from QDs that were stored in suspensions with their native ligands for several months; see the Supporting Information.

Our observed trend of increasing order of the Cd^{2+} ions with increasing radius and decreasing Cd/Se ratio is underscored by a concurrent decrease in the cadmium binding energy (see the Supporting Information). The average binding energy decreases because it is easier to ionize Cd coordinated to Se in the core of the QD than to ionize cadmium attached to the more electronegative O (in the form of Cd−OPA or Cd−PPA) on the surface of the QD.

SFG: The Density of Gauche Defects in the Ligand Shell Increases with Decreasing QD Radius. At sufficient surface coverages, bound alkyl chains will couple to each other via van der Waals forces (with a stabilization energy of ~2 kJ/mol/CH_2 group).[28,29] This stabilization is maximized for trans-extended alkyl chains, so intermolecular interactions promote the trans-extended conformation and inhibit the formation of gauche defects within the monolayer. To assess the extent of intermolecular order within the layer of OPA and PPA ligands coordinated to the QD surface, we determined the ratio of the SFG signal amplitudes of the symmetric methyl and methylene stretches $[E_{SFG}(CH_3,SS)/E_{SFG}(CH_2,SS)]$ of the alkyl groups that form the tails of the organic ligands through spectral fitting of the vibrational coherences. This SFG ratio is a well-established indicator of the density of gauche defects in alkyl chains because, as a coherent second order nonlinear spectroscopy, vibrational SFG is exquisitely sensitive to molecular symmetry.[30,31] A classic example is the strong SFG signal intensity originating from the asymmetric and symmetric CH stretches of the terminal methyl groups of well-ordered alkyl chains on a surface, which dominates the small or negligible SFG signal intensity originating from the asymmetric and symmetric CH stretches of the trans-configured methylene groups.[22,31,32] In general, as the alkyl chains become more disordered, the ratio $[E_{SFG}(CH_3,SS)/E_{SFG}(CH_2,SS)]$ decreases.[22,32−35]

Figure 2B shows representative SFG spectra of two sizes of CdSe QDs (R = 2.0 nm and R = 3.0 nm) spun-cast from hexane onto a glass slide, normalized to the maximum SFG intensity at 2875 cm^{-1}, and of a blank glass slide after hexane solvent evaporation. Figure 3C (black symbols) is a plot of the ratio of the SFG intensities of the symmetric methylene and symmetric methyl stretches (indicated with right and center vertical dashed lines in Figure 2B, respectively) from 90% TOPO CdSe QDs spun-cast onto a glass slide from hexane versus Cd/Se ratio and radius (inset). In general, as the QD radius decreases and the Cd/Se ratio increases, the SFG ratio $[E_{SFG}(CH_3,SS)/E_{SFG}(CH_2,SS)]$ decreases, and thus we conclude that the alkyl chains of the OPA and PPA ligands become increasingly disordered through formation of gauche defects. We note that the fractional surface coverage of phosphorus-containing ligands is approximately constant over this range of sizes of QDs (see the Supporting

dx.doi.org/10.1021/ja200466z |*J. Am. Chem. Soc.* 2011, 133, 7476–7481

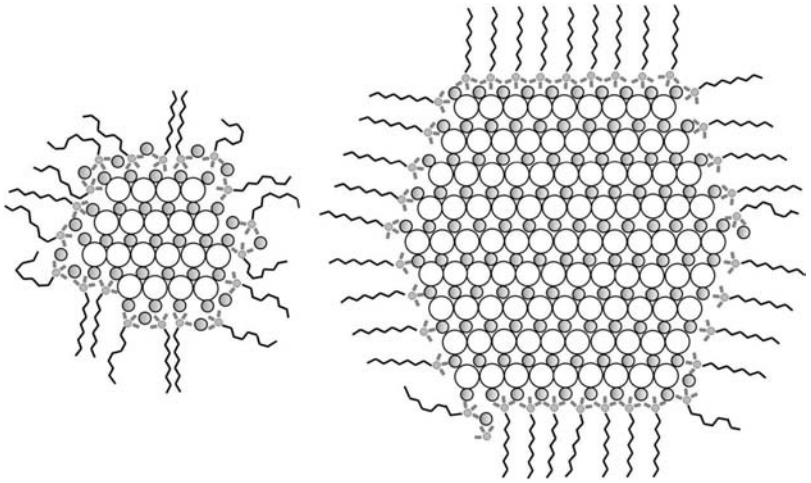

Figure 4. Schematic diagrams of proposed structures for a small QD with disordered Cd^{2+}−OPA shell (left), and a large QD with a more ordered CdSe surface that templates an ordered OPA monolayer (right). Within the ligands, gray circles are P atoms. Within the QD, white circles are Se^{2-}, and gray circles are Cd^{2+}.

Information). For reference, the vibrational SFG spectrum of the OPA ligand on a plain glass slide (no QDs present, see the Supporting Information) shows that the SFG signal amplitude from the methylene groups is dominated by that of the methyl stretches, which is consistent with the presence of well-ordered alkyl chains on the glass surface. Decreasing the QD radius also causes a decrease in the ratio of amplitudes of the asymmetric methyl stretching band (2940 cm^{-1}) to the symmetric methylene stretching band (2850 cm^{-1}); this trend is consistent with the interpretation that the alkyl chains of the organic ligands are less ordered for smaller QDs.

The ratio of SFG amplitudes decreases approximately monotonically when plotted against R (Figure 3C, inset), but its dependence on Cd/Se ratio appears to have two regimes: for Cd/Se < 2.6:1 (R > 2.4 nm), the SFG ratio decreases sharply as the Cd/Se ratio increases, but for Cd/Se > 2.6:1 (R < 2.4 nm), the SFG ratio has no apparent dependence on Cd/Se ratio. This result indicates that, for R > 2.4 nm, the disordering of the ligands is caused primarily by the disordering of the underlying Cd^{2+}, while for R < 2.4 nm, this surface-templated effect saturates, and the disordering of the ligands is due to another size-dependent parameter. We suspect that this parameter is the curvature of the QD surfaces, which can dictate the ligand order as follows: The curvature of the surface makes a cone volume available to the alkyl chains to explore a range of possible conformations. This cone volume increases, on average, with decreasing particle size. As suggested previously by SFG[20,22] and FTIR[21] measurements on alkyl chains bound to metal nanoparticles and roughened silica surfaces, intermolecular chain−chain interactions become less energetically favorable, and gauche defects begin to dominate the chain configuration as the particle size decreases. Additional molecular insight into this issue reported by Meulenberg, et al.[23] includes the notion that the average size of available continuous domains over which ligands can pack into thermodynamically stable configurations decreases with decreasing nanoparticle size. We observe that the radius at which the SFG ratio begins to depend exclusively on the size of the QD (and not its Cd/Se ratio), ∼2.4 nm, is very similar to the radius (2.2 nm) at which Meulenberg et al. observe that the domain size will begin to affect ligand ordering on faceted QD surfaces. The new insight presented here is that, above this critical radius, Cd enrichment creates a disordered layer that templates, and in fact amplifies, disorder in the ligands.

The red symbols in Figure 3C (inset) indicate the SFG ratios measured for samples of 99% TOPO QDs. We cannot use a direct comparison between the SFG data for 90% and 99% TOPO QDs to determine the role of cadmium enrichment in ligand disordering, as we did with the XPS measurements, because 90% TOPO QDs are passivated with OPA (an 8-carbon chain), and 99% TOPO QDs are passivated primarily with stearate (an 18-carbon chain); longer alkyl chains have more driving force to order within a film. Nonetheless, a comparison of the two data sets yields the expected result that, for a given radius, the stearate ligands on the 99% TOPO QDs were more ordered than the OPA ligands on the 90% TOPO QDs.

The results from our combined electron and coherent vibrational spectroscopy experiments on a range of sizes of CdSe QDs suggest that: (i) disorder in the chemical environment of Cd^{2+} ions, as detected by XPS, in the 90% TOPO CdSe QDs is due primarily to the presence of a disordered Cd^{2+}−OPA layer, which composes an increasing volume fraction of the QDs as they get smaller, and which is minimized or eliminated when the QDs are synthesized without OPA (i.e., with 99% TOPO); and (ii) disorder in the ligand layer, as detected by SFG, is templated by the disorder of the underlying Cd^{2+} layer for R > 2.4 nm and is probably dictated by the curvature of the QD surfaces for R < 2.4 nm. The latter could be due to either an increase in cone volume available to each ligand or a decrease in the size of available domains for ligand packing. Figure 4 shows graphical representations of the cross sections of our proposed structures for the smallest (most disordered) and largest (most ordered) QDs. The cartoons are drawn to scale with respect to the relative ionic radii of Cd^{2+} (95 pm), Se^{2-} (198 pm), and P (60 pm) and a C−C bond length of 147 pm. The O are represented as rectangles with lengths of 100 pm to indicate the potential for multiple, multidentate binding motifs.

■ CONCLUSIONS

The combination of XPS and SFG provides a detailed picture of the molecular mechanisms that control the intra- and

intermolecular order of organic ligands on the surface of small colloidal nanocrystals. The influence of both geometric and surface chemistry-related parameters on molecular order demonstrates the possibility for chemical control over this order by tuning the size of the QDs and the surfactant mixture used for their synthesis. The QD−OPA complex is a model system that is useful for testing the efficacy of the XPS−SFG strategy for investigating QD surfaces, and for discovering the operative mechanisms for ligand disordering in these systems. Importantly, however, the techniques and strategies we have outlined are applicable to QDs with conjugated ligands (which are more relevant for producing high-conductivity nanocrystal films). These strategies will enable exciting future exploration of the relationship between the intermolecular structure of ligands on nanoscopic surfaces and several properties of nanostructured hybrid materials, possibly including conductivity, surface passivation, and catalytic activity.

■ ASSOCIATED CONTENT

Supporting Information. Additional experimental details, ground-state absorption spectra of the QDs, XPS spectra of the QDs showing the P region, additional line width and binding energy data, data from control SFG experiments, a plot of the surface coverage of ligands on QDs, TEM diffraction patterns, and Figures S1−S7. This material is available free of charge via the Internet at http://pubs.acs.org.

■ AUTHOR INFORMATION

Corresponding Author
e-weiss@northwestern.edu; geigerf@chem.northwestern.edu

■ ACKNOWLEDGMENT

This work was supported by an Alfred P. Sloan Foundation Fellowship to F.M.G. and by the DOE through the Office of Science Early Career Research Award (DE-SC0003998) to E.A.W. K.E.K. is supported by a DOE Office of Science Graduate Fellowship. The TEM and XPS work was performed in the EPIC and KECK-II facilities of the NUANCE Center at Northwestern University. The NUANCE Center is supported by NSF-NSEC, NSF-MRSEC, Keck Foundation, the State of Illinois, and Northwestern University.

■ REFERENCES

(1) Miliron, D. J.; Hughes, S. M.; Yi, C.; Manna, L.; Jingbo, L.; Lin-Wang, W.; Alivisatos, A. P. *Nature* **2004**, *430*, 190–195.
(2) Konstantatos, G.; Howard, I.; Fischer, A.; Hoogland, S.; Clifford, J.; Klem, E.; Levina, L.; Sargent, E. H. *Nature* **2006**, *442*, 180–183.
(3) Ji, M. P.; Sungnam, C.; Stephen, T.; Mokari, T.; Cui, Y.; Gaffney, K. J. *Nano Lett.* **2009**, *9*, 1217–1222.
(4) Murray, C. B.; Kagan, C. R.; Bawendi, M. G. *Annu. Rev. Mater. Sci.* **2000**, *30*, 545–610.
(5) Huynh, W. U.; Dittmer, J. J.; Teclemariam, N.; Milliron, D. J.; Alivisatos, A. P.; Barnham, K. W. *Phys. Rev. B* **2003**, *67*, 115326.
(6) Sun, B. F.; Alp, T.; Sykora, M.; Werder, D. J.; Klimov, V. I. *Nano Lett.* **2009**, *9*, 1235–1241.
(7) Greenham, N. C.; Peng, X.; Alivisatos, A. P. *Phys. Rev. B* **1996**, *54*, 17628–17637.
(8) Loef, R. H.; Arjan, J.; Talgorn, E.; Schoonman, J.; Goossens, A. *Nano Lett.* **2009**, *9*, 856–859.
(9) Nelson, J.; Chandler, R. E. *Coord. Chem. Rev.* **2004**, *248*, 1181–1194.
(10) Nelson, J.; Haque, S. A.; Klug, D. R.; Durrant, J. R. *Phys. Rev. B* **2001**, *63*, 205321.
(11) Sharma, S. N.; Pillai, Z. S.; Kamat, P. V. *J. Phys. Chem. B* **2003**, *107*, 10088–10093.
(12) Huang, J.; Huang, Z.; Jin, S.; Lian, T. *J. Phys. Chem. C* **2008**, *112*, 19734–19738.
(13) Watson, D. F. *J. Phys. Chem. Lett.* **2010**, *1*, 2299–2309.
(14) Weiss, E. A.; Chiechi, R. C.; Kaufman, G. K.; Kriebel, J. K.; Li, Z.; Duati, M.; Rampi, M. A.; Whitesides, G. M. *J. Am. Chem. Soc.* **2007**, *129*, 4336–4349.
(15) Ji, X.; Copenhaver, D.; Sichmeller, C.; Peng, X. *J. Am. Chem. Soc.* **2008**, *130*, 5726–5735.
(16) Fritzinger, B.; Capek, R. K.; Lambert, K.; Martins, J. C.; Hens, Z. *J. Am. Chem. Soc.* **2010**, *132*, 10195–10201.
(17) Donakowski, M. D.; Godbe, J.; Sknepnek, R.; Knowles, K. E.; Olvera de la Cruz, M.; Weiss, E. A. *J. Phys. Chem. C* **2010**, *114*, 22526–22534.
(18) Ang, T. P.; Wee, T. S. A.; Chin, W. S. *J. Phys. Chem. B* **2004**, *108*, 11001–11010.
(19) Badia, A.; Cuccia, L.; Demers, L.; Morin, F.; Lennox, R. B. *J. Am. Chem. Soc.* **1997**, *119*, 2682–2692.
(20) Bordenyuk, A. N.; Weeraman, C.; Yatawara, A.; Jayathilake, H. D.; Stiopkin, I.; Liu, Y.; Benderskii, A. V. *J. Phys. Chem. C* **2007**, *111*, 8925–8933.
(21) Jones, R. L.; Pearsall, N. C.; Batteas, J. D. *J. Phys. Chem. C* **2009**, *113*, 4507–4514.
(22) Weeraman, C.; Yatawara, A. K.; Bordenyuk, A. N.; Benderskii, A. V. *J. Am. Chem. Soc.* **2006**, *128*, 14244–14245.
(23) Meulenberg, R. W.; Bryan, S.; Yun, C. S.; Strouse, G. F. *J. Phys. Chem. B* **2002**, *106*, 7774–7780.
(24) Qu, L.; Peng, Z. A.; Peng, X. *Nano Lett.* **2001**, *1*, 333–337.
(25) Morris-Cohen, A. J.; Donakowski, M. D.; Knowles, K. E.; Weiss, E. A. *J. Phys. Chem. C* **2009**, *114*, 897–906.
(26) Morris-Cohen, A. J.; Frederick, M. T.; Lilly, G. D.; McArthur, E. A.; Weiss, E. A. *J. Phys. Chem. Lett.* **2010**, *1*, 1078–1081.
(27) McBride, J. R.; Kippeny, T. C.; Pennycook, S. J.; Rosenthal, S. J. *Nano Lett.* **2004**, *4*, 1279–1283.
(28) Somasundaran, P.; Healy, T. W.; Fuerstenau, D. W. *J. Phys. Chem.* **1964**, *68*, 3562–3566.
(29) Ersoy, B.; Celik, M. S. *Clays Clay Mineral.* **2003**, *51*, 172–180.
(30) Shen, Y. R. *The Principles of Nonlinear Optics*; John Wiley & Sons: New York, 1984.
(31) Guyot-Sionnest, P.; Hunt, J. H.; Shen, Y. R. *Phys. Rev. Lett.* **1987**, *59*, 1597–1600.
(32) Hayes, P. L.; Keeley, A. R.; Geiger, F. A. *J. Phys. Chem. B* **2010**, *114*, 4495–4502.
(33) Esenturk, O.; Walker, R. A. *J. Chem. Phys.* **2006**, *125*, 174701.
(34) Conboy, J. C.; Messmer, M. C.; Richmond, G. L. *Langmuir* **1998**, *14*, 6722–6727.
(35) Stanners, C. D.; Du, Q.; Chin, R. P.; Cremer, P.; Somorjai, G. A.; Shen, Y.-R. *Chem. Phys. Lett.* **1995**, *232*, 407–413.
(36) Buchbinder, A. M.; Weitz, E.; Geiger, F. M. *J. Phys. Chem. C* **2010**, *114*, 554–566.
(37) Esenturk, O.; Walker, R. A. *J. Phys. Chem. B* **2004**, *108*, 10631–10635.
(38) Voges, A. B.; Al-Abadleh, H. A.; Musorrafiti, M. J.; Bertin, P. A.; Nguyen, S. T.; Geiger, F. M. *J. Phys. Chem. B* **2004**, *108*, 18675–18682.
(39) Stokes, G. Y.; Buchbinder, A. M.; Gibbs-Davis, J. M.; Scheidt, K. A.; Geiger, F. M. *J. Phys. Chem. A* **2008**, *112*, 11688–11698.
(40) Yu, W. W.; Qu, L.; Guo, W.; Peng, X. *Chem. Mater.* **2003**, *15*, 2854–2860.